frontiers | Frontiers in Energy Research

TYPE Original Research
PUBLISHED 22 November 2022
DOI 10.3389/fenrg.2022.899308

OPEN ACCESS

EDITED BY
Francesco Ciucci,
Hong Kong University of Science and Technology, Hong Kong SAR, China

REVIEWED BY
Aleksey Yaremchenko,
University of Aveiro, Portugal
Susana Garcia-Martin,
Complutense University of Madrid, Spain

*CORRESPONDENCE
Juliusz Dąbrowa,
dabrowa@agh.edu.pl

SPECIALTY SECTION
This article was submitted to Electrochemical Energy Conversion and Storage, a section of the journal Frontiers in Energy Research

RECEIVED 18 March 2022
ACCEPTED 04 November 2022
PUBLISHED 22 November 2022

CITATION
Dąbrowa J, Stępień A, Szymczak M, Zajusz M, Czaja P and Świerczek K (2022), High-entropy approach to double perovskite cathode materials for solid oxide fuel cells: Is multicomponent occupancy in (La,Pr,Nd,Sm,Gd)$BaCo_2O_{5+\delta}$ affecting physicochemical and electrocatalytic properties? *Front. Energy Res.* 10:899308. doi: 10.3389/fenrg.2022.899308

High-entropy approach to double perovskite cathode materials for solid oxide fuel cells: Is multicomponent occupancy in (La,Pr,Nd,Sm,Gd)$BaCo_2O_{5+\delta}$ affecting physicochemical and electrocatalytic properties?

Juliusz Dąbrowa[1]*, Anna Stępień[2], Maria Szymczak[1], Marek Zajusz[1], Paweł Czaja[3] and Konrad Świerczek[2,4]

[1]AGH University of Science and Technology, Faculty of Materials Science and Ceramics, Krakow, Poland, [2]AGH University of Science and Technology, Faculty of Energy and Fuels, Krakow, Poland, [3]Aleksander Krupkowski Institute of Metallurgy and Materials Science, Polish Academy of Sciences, Krakow, Poland, [4]AGH Centre of Energy, AGH University of Science and Technology, Krakow, Poland

High-entropy (La,Pr,Nd,Sm,Gd)$BaCo_2O_{5+\delta}$ double perovskite-type oxide having an equimolar, high-entropy, A-site-layered arrangement of cations is synthesized for the first time. A modified Pechini method, followed by calcination and sintering at 1,100°C helps in obtaining a single-phase, homogenous material with tetragonal *I4/mmm* symmetry. *In situ* X-ray diffraction and dilatometric studies show excellent phase stability up to 1,100°C in air, with the average thermal expansion coefficient of $23.7{\cdot}10^{-6}\ K^{-1}$ within the 25–1,100°C range. Total electrical conductivity of the metallic character exceeds 1,600 S cm^{-1} at room temperature. Equilibrated oxygen content at room temperature is determined as 5.69. The cathodic polarization resistance of the (La,Pr,Nd,Sm,Gd)$BaCo_2O_{5+\delta}$ layers, manufactured on the $La_{0.8}Sr_{0.2}Ga_{0.8}Mg_{0.2}O_{2.8}$ (LSGM) solid electrolyte of proved inertness, is as low as 0.037 Ω cm^2 at 900°C, and 0.175 Ω cm^2 at 750°C. The determined value of the power density in the LSGM-based, electrolyte-supported (thickness ca. 200 μm) fuel cell reaches 857 mW cm^{-2}. These results indicate possible applicability of the developed cathode material for solid oxide fuel cells, making it also one of the best-performing high-entropy air electrodes reported until now. However, the determined physiochemical characteristics of the material indicate a relatively limited influence of the high-entropy A-site arrangement in comparison to the conventional analogs, including the synthesized $Nd_{0.88}Sm_{0.12}Co_2O_{5+\delta}$ composition, characterized by the same effective radius of the lanthanide cations.

KEYWORDS

high-entropy oxides, double perovskites, cathode materials, electrocatalytic activity, solid oxide fuel cells

1 Introduction

In the era of growing energy demand, the importance of green-energy conversion technologies cannot be overestimated. Among the proposed new approaches, Solid oxide fuel cells (SOFC) technology is of special interest, offering improved efficiency, not only in terms of electricity production but also through possible utilization of the concurrently produced heat (Larminie and Dicks, 2003). If fueled by hydrogen, the level of pollution generated by SOFCs is negligible, and even more importantly, the possibility of the reversible operation, i.e., work in the high-temperature electrolysis mode, which can be realized in the reversible solid oxide cells (rSOC), brings about unprecedented possibilities for supporting the power-grid balance (Ramadhani et al., 2017), making SOFC technology one of the most appealing opportunities regarding the development of the Power-to-X (P2X) technologies (Boaro, 2014; Gao et al., 2016). While finally, it seems that the broader commercial application of SOFCs is indeed taking place (Staffell et al., 2019), the technology remains limited by certain unresolved issues among which are still too high-operating temperature, long-term performance stability, as well as high manufacturing and operating costs should be listed (Mahato et al., 2015; Zhao et al., 2017).

As of today, the biggest performance losses for SOFC cells operating at reduced temperatures (<800°C) can be associated with cathodic polarization resistance (Boaro, 2014). This is mainly due to the insufficiently low catalytic activity toward the oxygen reduction reaction (ORR) (Ishihara, (2014) *Perovskite Oxide for Solid Oxide Fuel Cells* New York: Springer). Currently developed state-of-the-art air electrode materials, while delivering a largely improved performance, are still troubled by a number of crucial problems related to insufficient chemical and microstructural stability, unsuitable thermomechanical characteristics, and vulnerability to CO_2- and Cr-poisoning effects (Fergus, 2005; Gao et al., 2016).

Among the most promising cathode materials, the so-called double perovskites with the chemical formula of $REBaCo_2O_{5+\delta}$ (RE: La, Pr, Nd, Gd, Sm, Y, etc.), also including partially doped materials, must be mentioned (Raveau and Seikh, (2012); Karppinen et al., 2002; Frontera et al., 2005; Raveau and Seikh, (2012); Mogni et al., 2013; Volkova et al., 2013; Pelosato et al., 2015). The uniquely layered arrangement in the RE-Ba sublattice, which is directly influencing structural, transport, as well as electrocatalytic properties, enables manufacturing of air electrode layers showing excellent catalytic activity toward ORR (Kim and Manthiram, 2008; Kim et al., 2012; Sengodan et al., 2015). This is mainly due to the high mixed ionic–electronic conductivity (MIEC), especially with regard to the ionic contribution, as well as the presence of catalytically-active cobalt cations at the surface region with coordination number lower than six (Kim and Manthiram, 2015; Hwang et al., 2017). What is more, the high versatility of double perovskites allows for the application not only in SOFCs but also in Protonic Ceramic Fuel Cells (PCFC) (Kim and Manthiram, 2015). Still, the considered materials exhibit some disadvantages, such as relatively high values of the thermal expansion coefficient (TEC), limited chemical stability at the interface with solid electrolytes, vulnerability to CO_2 from the atmosphere, as well as to the previously mentioned Cr-poisoning from the interconnects (Sun et al., 2010). However, it is believed that at least some of those problems can be addressed by proper doping (Liu et al., 2017).

While doping at the B-site of Co-based double perovskites (e.g., with Fe, Mn, or Cu) has been relatively thoroughly studied (Karppinen et al., 2002; Zhang, 2004; Tsvetkov et al., 2011; Kim et al., 2013; Broux et al., 2014; Tsvetkov et al., 2016; Kong, 2018; Olszewska and Świerczek, 2019; Olszewska et al., 2019), in the case of this type of double perovskites, the occupancy of the A-sites can have an equally great impact on the properties of the materials, creating further opportunities for their tailoring. In fact, most of the properties, such as oxygen non-stoichiometry, electronic conductivity, ionic conductivity, or thermal expansion coefficient (TEC), can be directly correlated to the ionic radius of the A-site lanthanide and/or its difference when compared to Ba cations, see also Supplementary Figure S1 (Lee et al., 1998; Du et al., 2014; Kim and Manthiram, 2015; Olszewska, Świerczek, et al., 2019). In most cases, the selection of bigger RE ions, such as La or Pr, helps in enhancing the transport properties, however, at a price of increasingly high TEC values (Kim and Manthiram, 2015) (e.g., from 18.2 to $29.5{\cdot}10^{-6}$ K^{-1} for $YBaCo_2O_{5+\delta}$ and $LaBaCo_2O_{5+\delta}$, respectively) (Olszewska, Świerczek, et al., 2019) Similarly, the oxygen nonstoichiometry also changes drastically, varying at room temperature from $\delta \approx 0.41$ to $\delta \approx 1$ for Y- and La-based compositions, respectively, and can be further modified by substituting Ba with other smaller alkali ions such as Sr or Ca (Kim and Manthiram, 2015). However, despite the profound effect of the A-site occupancy on the properties of the double perovskites, the studies concerning the utilization of multi-ionic A-site arrangement (with multiple lanthanide ions) are still much less popular than those of B-site modifications. In this context, it seems that one especially tempting, but yet not explored, approach for further adjustment of the physicochemical and electrochemical properties of double perovskites is to apply the high-entropy design principle. This way offers a number of additional potential

advantages, such as increased stability due to the entropic stabilization, and potentially, the presence of additional synergistic effects (Miracle and Senkov, 2016; Kübel et al., 2018). In this context, based on the aforedescribed profound impact of the relationship between Ba and RE ions' ionic radii, it still remains to be seen whether the inherent lattice distortion and spread of the ionic radii in the high-entropy compound might introduce further, unexpected effects, thanks to replacing the atomic-level smooth Ln-O plane by a highly distorted, uneven, high-entropy analog, in which the ionic radius of the lanthanide changes from one lattice site to another.

The application of the high-entropy approach to design novel oxide systems led to the development of the high-entropy oxides (HEOx) family, which since the pioneering study of Rost *et al.* in 2015 concerning the rock salt-structured (Co,Cu,Mg,Ni,Zn)O (Vinnik, et al., 2019), has been expanded on a vast number of compositions and structures, including the high-entropy perovskites Zhang et al. (2019) *History of high entropy oxides*, Singapore: Spronger Nature; Djenadic et al., 2016; Berardan et al., 2016; Li et al., 2019; Tseng and Mccormack, 2019; Vinnik et al., 2019; Dąbrowa et al., 2020a; Dąbrowa et al., 2021). Despite a very short development history, such materials have already been proven to exhibit a number of potentially interesting features from the viewpoint of SOFC technology. For example, in our previous article, it was documented that Cr-containing $La_{1-x}Sr_x(Co,Cr,Fe,Mn,Ni)O_{3-\delta}$ (x = 0, 0.1, 0.2, 0.3) simple perovskite could be successfully used as the air electrode material for SOFCs (Dąbrowa et al., 2020b), displaying a number of beneficial, functional features such as moderate thermomechanical behavior and high-temperature stability. Another recent report concerning the high-entropy equivalent of the LSM material ($La_{1-x}Sr_xMnO_{3-\delta}$), namely the $(La,Nd,Pr,Sm,Sr)MnO_{3-\delta}$, showed that the utilization of the high-entropy design principle with regard to the "A" sublattice may allow suppressing the alkaline ions surface segregation, greatly enhancing the longevity of the fuel cell (Yang et al., 2021), a feature which might also be of interest in double perovskites, suffering from the similar issue (Kim et al., 2009a). Last, but not least, in nearly all known cases, not only regarding the SOFC applications (Han et al., 2021; Shen et al., 2021) but other energy-conversion technologies as well (Kübel et al., 2018; Zhao et al., 2020), HEOx are characterized by excellent long-term stability of electrochemical performance, an effect whose origins still remains far from being completely understood.

Considering the aforementioned benefits of the high-entropy approach, as well as the lack of reports regarding the possibility of obtaining high-entropy double perovskites, not to mention their possible application in SOFCs, it is especially appealing to evaluate the properties of the proposed $(La,Pr,Nd,Sm,Gd)BaCo_2O_{5+\delta}$ material. This is particularly of interest since, as was described earlier, the ionic radius (or mean radius) of the lanthanides strongly influences the physiochemical characteristics of the double perovskites (Kim and Manthiram, 2008; Kim J. H. et al., 2009; Kim and Manthiram, 2015). However, it remains an open question as to whether by the introduction of the high-entropy approach at the A-site, these properties can be affected beyond the simple interpolation based upon the mean radius of all introduced lanthanides. Therefore, to provide a valid reference, a more conventional $Nd_{0.88}Sm_{0.12}Co_2O_{5+\delta}$ composition was also prepared with the ratios of the lanthanide ions being selected to provide an identical effective ionic radius, but without the level of lattice distortion, typically associated with the high-entropy compounds.

2 Materials and methods

The studied materials, namely $La_{0.2}Pr_{0.2}Nd_{0.2}Sm_{0.2}Gd_{0.2}BaCo_2O_{5+\delta}$ [later denoted as $(La,Pr,Nd,Sm,Gd)BaCo_2O_{5+\delta}$] and $Nd_{0.88}Sm_{0.12}Co_2O_{5+\delta}$, were synthesized by using a modified Pechini method, using nitrate precursors provided by Alfa Aesar (99.9% purity for lanthanide salts, 98–102% for cobalt nitrate). Citric acid monohydrate (Alfa Aesar 99.5+ %) and ethylene glycol (EG) were also used, with the molar ratio of all the cations, citric acid, and EG in the mixture being 1:2:4. After dissolving in demineralized water, the mixture was then put on a magnetic stirrer, with a heating plate set initially to 150°C (esterification step). After obtaining a clear solution, the temperature was increased to 300°C. The obtained gel was calcined at 800°C for 4 h to remove organics, and then at 1,100°C for 16 h to decompose the highly-stable barium carbonate. This step was followed by slow cooling (with the furnace) to room temperature (RT). The obtained powder after grounding was used to prepare pellets of 10 mm in diameter, formed under a repeatedly applied pressure of 1, 1.5, and 2 tons, using a uniaxial hydraulic press with a vacuum pump attached. Subsequently, the green pellets were free-sintered in a chamber furnace for 20 h at 1,200°C, and cooled at the rate of 2°C min^{-1} to ensure close-to-equilibrium oxygen content and decrease the possibility of cracking.

The X-ray diffraction (XRD) measurements were performed at RT using a Panalytical Empyrean diffractometer with Cu Kα radiation, working in Bragg–Brentano geometry, within a 10–90 deg range. The obtained data were analyzed with the GSAS/EXPGUI set of software on a basis of Rietveld refinements. Structures at high temperatures and the corresponding TEC values were investigated using results from the high-temperature (HT) XRD measurements carried out on an Anton Paar HTK 1200N oven-chamber mounted on the diffractometer. The thermal expansion data were further supplemented by dilatometric measurements using a Linseis L75 Platinum Series dilatometer.

Morphology, chemical composition, and homogeneity of the materials were studied by scanning electron microscopy (SEM) combined with the energy-dispersive X-ray spectroscopy (EDS), using ThermoFisher Scientific Phenom XL Desktop SEM equipped with a silicon drift detector. The applied voltage for EDS analysis was 15 kV. The results were processed with the use of ProSuite software.

Further evaluation of the chemical and structural homogeneity of the studied high-entropy double perovskite was performed on the La,Pr,Nd,Sm,Gd)$BaCo_2O_{5+\delta}$ pellet (free-sintered in a chamber furnace for 20 h at 1,200°C, and cooled at the rate of 2°C min^{-1}), using the transmission electron microscopy (TEM). Thin lamellae for the TEM investigation were prepared using Thermo-Fisher Scientific SCIOS II DUAL BEAM scanning electron microscope. TEM and Scanning TEM (STEM) measurements were carried out using Thermo-Fisher Scientific Titan Themis XFEG 200 kV S/TEM, equipped with a probe Cs-corrector.

The oxygen content in the synthesized materials was established with the iodometric titration method (Olszewska et al., 2018). The end-point of the titration was detected potentiometrically with an EM40-BNC Mettler Toledo titrator. The whole process was carried out in an argon atmosphere, and deionized water, used as a titration medium, was previously freed from the dissolved oxygen by boiling. To ensure the removal of the adsorbed species on the powdered material, immediately before iodometric titration, the sample was heated up to 200°C in air and then slowly cooled to RT. In order to evaluate the oxygen content changes with temperature, the thermogravimetric (TG) method was utilized (TA Q5000 IR thermobalance) with measurements (two consecutive cycles) performed in synthetic air in an RT-900°C temperature range, with 5°C min^{-1} heating and cooling rates.

Electrical conductivity studies by the 4-probe DC method were conducted within a temperature range of 25–1,000°C, using the Fine Instruments FRASB-1000 setup consisting of: TF1200 tube furnace, Keysight Multimeter 34465A, Keysight Function/Arbitrary Waveform Generator 33210A, control unit CFRASB-1000 with AM16/32B multiplexer, measuring probe SSC-15, and BR07 retaining decade.

To measure the cathodic polarization resistance, LSGM ($La_{0.8}Sr_{0.2}Ga_{0.8}Mg_{0.2}O_{3-\delta}$) electrolyte-supported symmetric cells with (La,Pr,Nd,Sm,Gd)$BaCo_2O_{5+\delta}$|LSGM|(La,Pr,Nd,Sm,Gd)$BaCo_2O_{5+\delta}$ configuration were prepared and tested. Dense electrolyte pellets with a thickness of approx. 600 μm were sintered using commercial LSGM powder (Fuelcellmaterials), homogeneously mixed with 1 wt % of the poly(vinyl butyral-co-vinyl alcohol-co-vinyl acetate). The mixture was pressed into 13 mm diameter pellets and annealed in air at 1,450 °C. Screen printing was used to manufacture electrode layers on both sides of the electrolyte. This required preparing the electrode slurry by mixing fine (*i.e.*, as-sintered) (La,Pr,Nd,Sm,Gd)$BaCo_2O_{5+\delta}$ powder with a commercial texanol-based binder (ESL ElectroScience) in a 2:1 wt. ratio, with 5 wt% addition of a pore-forming agent (starch). Sintering of the layers was performed at 1,100°C for a duration of 2 h.

Electrochemical properties of the constructed symmetrical cells were determined by electrochemical impedance spectroscopy (EIS) using the Solartron 1,260 Frequency Response Analyzer, combined with 1,287A electrochemical interface. Data were measured in the temperature range of 600–900°C. Studies were performed in the 0.1–10^6 Hz range with a perturbation amplitude signal of 25 mV. For data-fitting, an L-R_0-Q_1R_1-Q_2R_L equivalent circuit was used (analyzed with the ZView software). For details about the interpretation of the respective resistances (R) and meaning of the constant phase elements (Q), see previous works (Zhao et al., 2013; Du et al., 2014; Zhang et al., 2015; Du et al., 2017).

In addition, an electrolyte-supported (thickness ca. 200 μm) button-type full cell with Ni-$Ce_{0.8}Gd_{0.2}O_{2-\delta}$|$Ce_{0.8}Gd_{0.2}O_{2-\delta}$|$La_{0.8}Sr_{0.2}Ga_{0.8}Mg_{0.2}O_{3-\delta}$|(La,Pr,Nd,Sm,Gd)$BaCo_2O_{5+\delta}$ configuration was prepared. Due to the known poor chemical stability between Ni and LSGM electrolytes on the anode side of the asymmetrical cell, a $Ce_{0.8}Gd_{0.2}O_{2-\delta}$ (gadolinium-doped ceria, GDC; fuel cell materials) buffer layer was applied with the screen-printing method, followed by sintering at 1,300°C for 2 h. Afterward, an Ni–GDC cermet

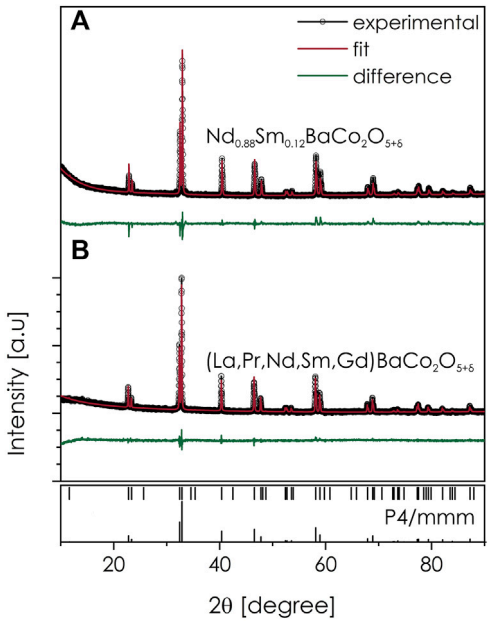

FIGURE 1
Diffractogram measured at RT for the as-calcined powders of Ba(La,Pr,Nd,Sm,Gd)$Co_2O_{5+\delta}$ and $Nd_{0.88}Sm_{0.12}Co_2O_{5+\delta}$, together with Rietveld refinement.

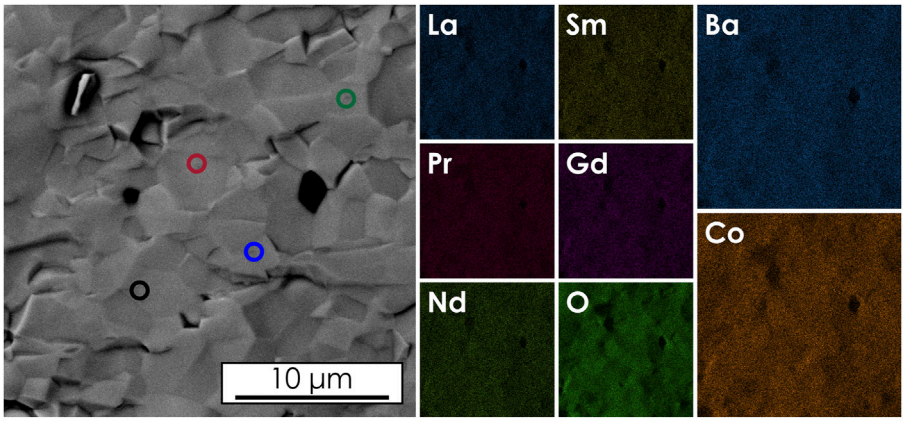

	La	Pr	Nd	Sm	Gd	Ba	Co	O
○	3.8	5.5	3.8	2.7	4.2	14.1	20.8	45.1
○	3.1	4.9	3.5	2.7	4.3	13.8	20.6	47.1
○	3.4	5.3	3.9	3.2	3.9	14.9	21.6	43.8
○	3.4	5.2	3.6	3.0	4.1	14.6	20.8	45.3

FIGURE 2
Micrograph taken from a fractured (La,Pr,Nd,Sm,Gd)$BaCo_2O_{5+\delta}$ pellet. Results of the EDS mappings and point analysis data (at% values) are also provided.

anode (with an initial NiO to GDC wt. ratio of 60:40) was applied and sintered at 1,350°C for 2 h. Then, the (La,Pr,Nd,Sm,Gd)$BaCo_2O_{5+\delta}$ layer was screen-printed on the cathode side of the cell and sintered at 1,100°C. The Ag paste was used to prepare the current collectors, with its sintering temperature equal to 750°C. During tests, humidified hydrogen (3 vol% of H_2O) with a 40 cm^3/min flow rate was supplied to the anode, and air with a 100 cm^3/min flow rate was supplied to the cathode.

3 Results and discussion

3.1 Comparison of physicochemical properties of (La,Pr,Nd,Sm,Gd)$BaCo_2O_{5+\delta}$ in relation to $REBaCo_2O_{5+\delta}$

As visible in Figure 1, the measured diffractogram for the calcined powders of both (La,Pr,Nd,Sm,Gd)$BaCo_2O_{5+\delta}$ and $Nd_{0.88}Sm_{0.12}Co_2O_{5+\delta}$ show a typical set of peaks corresponding to the double perovskite (A-site layered) crystal structure, with no secondary phase reflexes visible, confirming the phase purity. Rietveld refinement of the data allowed to confirm the presence of aristotype, tetragonal *P*4/*mmm* space group in both compositions, with the RT lattice cell parameters equal to a = 3.9014(1) and c = 7.6123(1) Å, and a = 3.9020(1) and c = 7.6060(1) Å, for (La,Pr,Nd,Sm,Gd)$BaCo_2O_{5+\delta}$ and $Nd_{0.88}Sm_{0.12}Co_2O_{5+\delta}$, respectively, with a good agreement between these values proving the correctness of the conventional composition's design. After sintering, the materials preserved their single-phase structure, see Supplementary Figure S2. Importantly, for this refinement, preferential orientation had to be included to obtain the matching intensity of the fitted profile to the measured data. This is expected for the measurements of the sintered pellet comprising the layered oxide material.

In order to evaluate the potential benefits of the high-entropy approach application, it is necessary to place the obtained experimental data in the proper context. As already mentioned, in the double perovskites, the size of the lanthanides plays a crucial role in terms of the material's properties, therefore, it can be expected that by determining the effective mean radius of the RE cations in high-entropy double perovskites, one will be able to interpolate the expected values of physiochemical parameters, not accounting for the possible synergies. Regarding the mean value of the (effective) radius $\bar{r}$ of all the employed RE cations, utilizing Shannon radii data and considering 8-fold coordination, it can be calculated as 1.105 Å for both (La,Pr,Nd,Sm,Gd)$BaCo_2O_{5+\delta}$ and $Nd_{0.88}Sm_{0.12}Co_2O_{5+\delta}$, placing these materials between the Nd^{3+}- (1.109 Å) and Sm^{3+}-based compositions (1.079 Å) (Shannon, 1976). With this value and the known unit cell parameters for $NdBaCo_2O_{5+\delta}$ and $SmBaCo_2O_{5+\delta}$ materials obtained in the same synthesis route (Olszewska et al., 2018), the expected

10.3389/fenrg.2022.899308

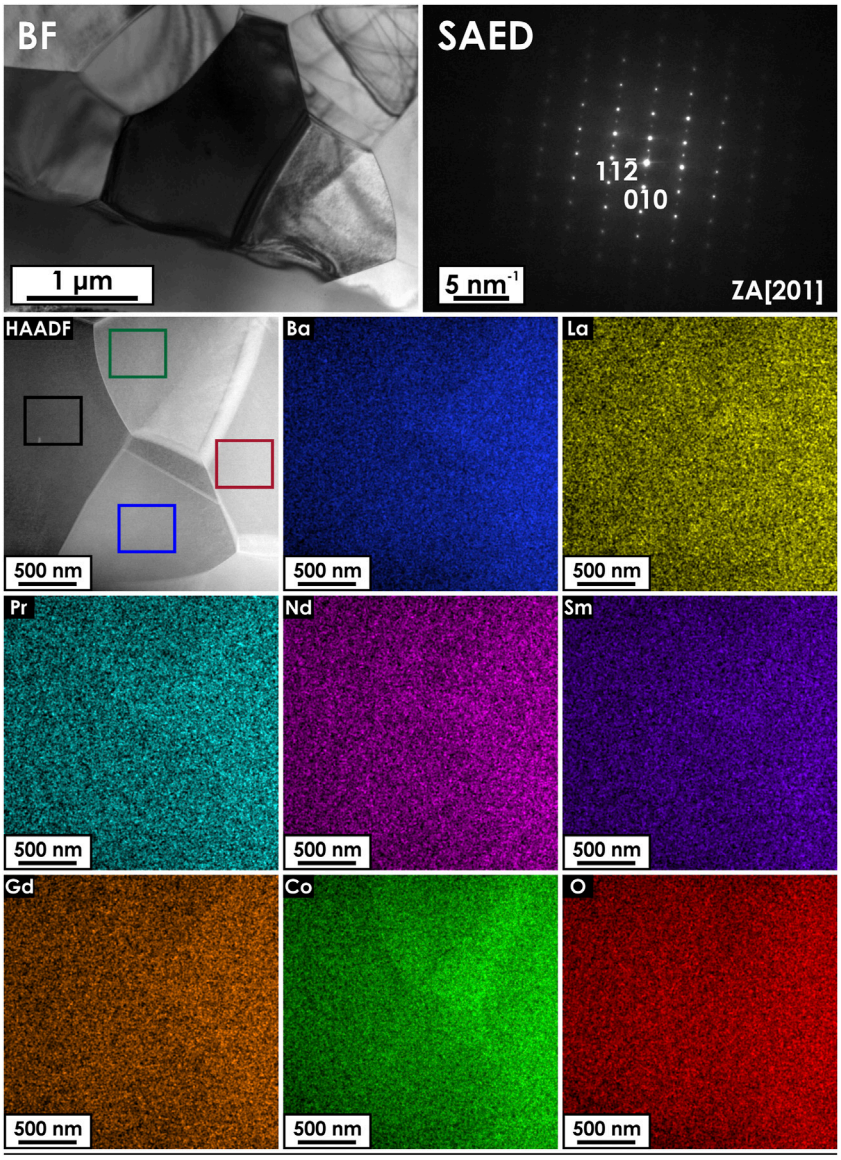

	La	Pr	Nd	Sm	Gd	Ba	Co	O
☐	2.1	2.1	2.1	2.0	1.9	10.3	22.7	56.5
☐	2.1	2.0	2.2	1.8	1.7	9.5	20.9	59.8
☐	1.9	1.8	2.1	1.8	1.7	9.2	21.7	59.8
☐	1.8	1.8	2.2	1.8	1.6	8.9	20.7	61.3

FIGURE 3
Exemplary bright field image (upper left-hand corner) and the corresponding SAED pattern (upper right-hand corner), taken from a thin lamella of the (La,Pr,Nd,Sm,Gd)BaCo2O5+δ sample. The zone axis (ZA) along which the SAED pattern was taken is indicated. The lower part of the figure presents the results of STEM/EDS mapping, with the corresponding elemental distribution maps across the studied area. The results of the EDS analysis in typical micro areas in four different grains are also provided (at%).

values of a and c parameters, as well as volume V_{cell} can be derived, which are very close to the actual, measured data for both studied materials (Supplementary Table S1).

Regarding the homogeneity and microstructure of the considered high-entropy double perovskite, results from the SEM/EDS analyses of the fractured pellet, presented in

Figure 2, indicate even and close-to-nominal content of the elements in the sample. Furthermore, the sinter is characterized by high density. Considering the EDS point-analysis data, it should be remembered that for the lanthanide cations, the overlapping of the EDS signal occurs which hinders the sensitivity of the method to evaluate with respect to rare-earth elements. Nevertheless, it can be stated that within the expected accuracy range, the results confirm the homogeneity of the obtained sample.

While based on the XRD and SEM/EDS data it can be stated that the studied (La,Pr,Nd,Sm,Gd)$BaCo_2O_{5+\delta}$ material is homogenous and single-phase, it should be noted that in the case of $REBaCo_2O_{5+\delta}$ double perovskites the atomic-scale behavior is often complex, exhibiting a tendency toward the presence of local domains, which can be described by different space groups (Muñoz-Gil et al., 2014). Such effects may be correlated with the local differences in the oxygen non-stoichiometry level, which in turn might affect the properties of the material. In order to verify chemical and structural homogeneity TEM observations were carried out for multiple regions and grains within the prepared lamellae. First, the analysis was performed in TEM mode. A number of bright field images (BF) together with the corresponding selected area electron diffraction patterns (SADP) were taken from different grains. The exemplary results are presented in Figure 3. According to SADPs, the sample is homogenous and the phase structure is well-indexed according to the *P4/mmm* structure with SADPs taken along the [201], [$\bar{2}$21], and [$\bar{4}$61] zone axes (Figure 3 and Supplementary Figure S3). The phase indexing was done by comparing the software-simulated SADPs of the expected phase with experimental ones, with the obtained level of agreement equal to 100%. On top of the structural analysis, STEM-high-angle annular dark-field (HAADF) analysis coupled with EDS elemental distribution mapping was also conducted, see Figure 3 and Supplementary Figure S4. From the EDS maps taken, as well as the results of the EDS area analysis, it is clear that the elemental distribution is uniform and consistent with the nominal composition. On the whole, a detailed high-resolution S(T)EM analysis confirms the homogeneity of the studied material, which is further confirmed by a high-resolution HRTEM image (Supplementary Figure S5).

Based on the HT-XRD measurements it can be stated that the (La,Pr,Nd,Sm,Gd)$BaCo_2O_{5+\delta}$ material is stable within the 25–1,100°C range in air, with the corresponding thermal expansion coefficient (TEC) value being $19.7(6)\cdot10^{-6}$ and $25.2(1)\cdot10^{-6}\ K^{-1}$ for 25–400°C and 400–1,000°C ranges, respectively (see Supplementary Table S2 and Supplementary Figures S6, S7A). These results are also in perfect agreement with the TEC values determined for the respective temperature ranges with the use of dilatometric measurements determined as $19.7(1)\cdot10^{-6}\ K^{-1}$ and $25.2(1)\cdot10^{-6}\ K^{-1}$ (Supplementary Figure S7B). A closer comparison with the effective thermal expansion reported for $NdBaCo_2O_{5+\delta}$ ($25.1(1)\cdot10^{-6}\ K^{-1}$ for 400–900°C) and $SmBaCo_2O_{5+\delta}$ ($23.1(1)\cdot10^{-6}\ K^{-1}$ for 400–900°C) reveals that the recorded TEC value is just slightly higher than the expected one, calculated as a weighted average from the aforementioned values (i.e., $24.8(1)\cdot10^{-6}\ K^{-1}$). What is, however, very interesting, is that the more conventional $Nd_{0.88}Sm_{0.12}Co_2O_{5+\delta}$ composition appears to be characterized by slightly lower TEC values of 19.1(1) and $23.7(1)\cdot10^{-6}$ K¯1, suggesting that the averaging of properties in the high-entropy composition might actually be even more effective. In terms of the particular lattice parameters, the comparison of the thermal expansion of *a* and *c/2* parameters in (La,Pr,Nd,Sm,Gd)$BaCo_2O_{5+\delta}$ with the data for Nd- and Sm-based double perovskites is presented in Supplementary Figure S8, with a similar comparison for the unit cell's volume being shown in Supplementary Figure S9. Generally, it can be stated that the observed thermal expansion behavior of (La,Pr,Nd,Sm,Gd)$BaCo_2O_{5+\delta}$ closely matches the one reported for conventional $REBaCo_2O_{5+\delta}$ double perovskites, being, as expected, very close to the one of $NdBaCo_2O_{5+\delta}$ with a significant chemical expansion component appearing at elevated temperatures (Kim and Manthiram, 2008; Zhang et al., 2008).

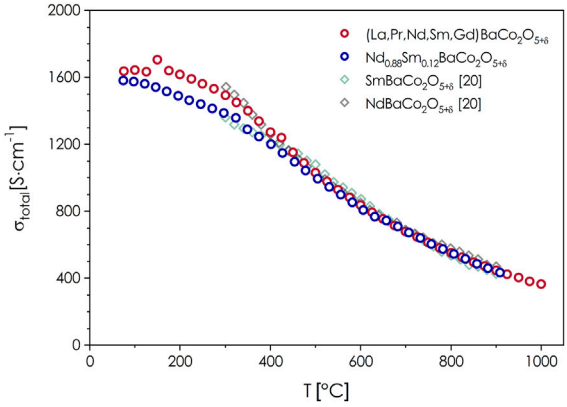

FIGURE 4
Temperature dependence of the total electrical conductivity in air determined for a dense pellet of (La,Pr,Nd,Sm,Gd)$BaCo_2O_{5+\delta}$ with the use of the 4-probe DC method. Reference data for $NdBaCo_2O_{5+\delta}$ and $SmBaCo_2O_{5+\delta}$ from (Kim and Manthiram, 2015).

The total electrical conductivities of (La,Pr,Nd,Sm,Gd)$BaCo_2O_{5+\delta}$ and $Nd_{0.88}Sm_{0.12}Co_2O_{5+\delta}$ materials, measured as a function of temperature, are shown in Figure 4. Reference plots for $NdBaCo_2O_{5+\delta}$ and $SmBaCo_2O_{5+\delta}$ are also provided (Kim and Manthiram, 2015). As typical behavior for Co-based double perovskites, the materials exhibit a metallic-type conductivity behavior, with exceptionally high specific-conduction values, which in the vicinity of RT exceed 1,600 S cm^{-1}. These results are consistent with a high degree of electronic delocalization, which occurs only if favorable conditions for the electronic

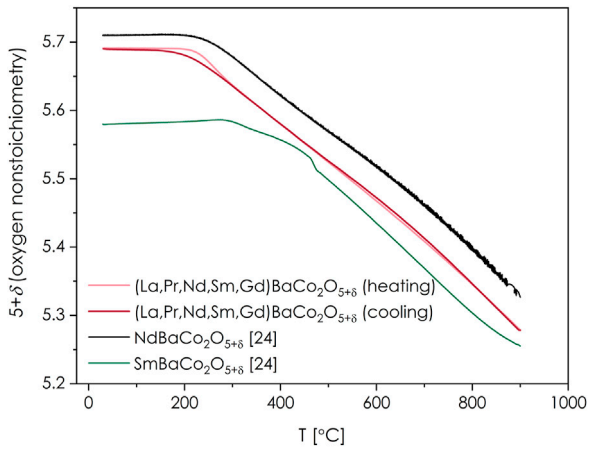

FIGURE 5
Temperature dependence of close to equilibrium oxygen content in $(La,Pr,Nd,Sm,Gd)BaCo_2O_{5+\delta}$ as determined by iodometric titration (initial data at RT) and TG measurements during both heating and cooling runs. Reference data for $NdBaCo_2O_{5+\delta}$ and $SmBaCo_2O_{5+\delta}$ are also included (Olszewska et al., 2018).

conduction appear (Co-O-Co bond angles being equal to 180 deg in the aristotype *P4/mmm* structure, and limited oxygen vacancies concentration near RT). At elevated temperatures, the behavior is strongly correlated with the oxygen release from the structure (see below), leading to the increased oxygen vacancies content. This may be interpreted as originating from disruption of the Zener double-exchange mechanism (Goodenough, 1958), but can be also understood as due to the decreased concentration of the effective charge carriers (electron holes) (Olszewska et al., 2018). Furthermore, with the chemical expansion taking place, less effective overlapping between O 2*p* and Co 3*d* orbitals must also be mentioned as a factor influencing electrical conductivity behavior at elevated temperatures. Considering the comparison to conventional double perovskites with RE = Nd or Sm, the conductivity values are very similar to the ones reported for $NdBaCo_2O_{5+\delta}$ and slightly higher than in $SmBaCo_2O_{5+\delta}$ up to ca. 400°C (for reference to other double perovskites also see Supplementary Figure S1A). In comparison, the behavior of $Nd_{0.88}Sm_{0.12}Co_2O_{5+\delta}$, especially within the 100–400 °C, is more similar to $SmBaCo_2O_{5+\delta}$. Above this threshold, the behavior of all four considered compositions is nearly identical (Kim and Manthiram, 2015). It is worth noting that the possible distortion of the lanthanide sublattice, resulting from the presence of different-sized RE ions, does not affect the effectiveness of the charge transfer.

In order to fully understand the transport properties of $(La,Pr,Nd,Sm,Gd)BaCo_2O_{5+\delta}$, knowledge of the actual, equilibrated oxygen content as a function of temperature must be provided. Consequently, oxygen nonstoichiometry, essential for the physiochemical properties, was established at RT using the iodometric titration method. The equilibrium oxygen content was found to be 5.69, which is almost the same as the anticipated (interpolated) value considering the trend in the $REBaCo_2O_{5+\delta}$ series (Supplementary Figure S1C, Supplementary Table S3). In the case of $Nd_{0.88}Sm_{0.12}Co_2O_{5+\delta}$, a slightly higher value of $\delta = 0.71$ was determined, which is still comparable within the assumed error of the method. The obtained value of $\delta = 0.69$ is slightly smaller than Pr- and Nd-containing materials (0.85 and 0.78 (Kim and Manthiram, 2015), respectively, or 0.77 and 0.70 (Olszewska et al., 2018), depending on the applied methodology), while, in line with the expectations, it is bigger than that in the case of $SmBaCo_2O_{5+\delta}$ [0.65 (Kim and Manthiram, 2015) or 0.58 (Olszewska et al., 2018)]. The observed agreement with the rule of mixture predictions must be emphasized because of the high sensitivity of the double perovskite structure toward this parameter. It should be noted that observing at RT *P4/mmm* tetragonal symmetry of $(La,Pr,Nd,Sm,Gd)BaCo_2O_{5+\delta}$ and $Nd_{0.88}Sm_{0.12}Co_2O_{5+\delta}$ corresponds to the vacancy-disordered structure, and similarly for slightly bigger Nd ions, but contrary to the *Pmmm* symmetry with δ close to 0.5 as observed for $SmBaCo_2O_{5+\delta}$ (Olszewska et al., 2018).

The determined RT value is then taken as a starting point for the TG measurements in air, allowing to present the temperature dependency of the oxygen content in $(La,Pr,Nd,Sm,Gd)BaCo_2O_{5+\delta}$, as presented in Figure 5. For comparison, again, the data for $NdBaCo_2O_{5+\delta}$ and $SmBaCo_2O_{5+\delta}$ are also provided (Olszewska et al., 2018). Unfortunately, due to technical limitations, it was not possible to perform such measurements for the $Nd_{0.88}Sm_{0.12}Co_2O_{5+\delta}$ composition. The observed level of the oxygen release at 900°C with δ decreasing down to 0.28 is probably the only distinctive feature of $(La,Pr,Nd,Sm,Gd)BaCo_2O_{5+\delta}$, which does not follow the expected (interpolated) behavior compared to the reported RE = Nd and Sm compounds (Olszewska et al., 2018). While it is still in between the results for both mentioned compositions within the considered temperature range, the curve of oxygen release, which starts much closer to the one for Nd-containing perovskite, ends up closer to the Sm-containing one at 900°C. This larger-than-anticipated oxygen release might be due to the presence of a significant amount of bigger RE^{3+} cations (La and Pr), for which Co-based double perovskites tend to release oxygen more strongly and at lower temperatures (Olszewska et al., 2018).

3.2 Electrochemical performance as the candidate air electrode material

With only marginal differences in the physicochemical characteristics of the high-entropy $(La,Pr,Nd,Sm,Gd)BaCo_2O_{5+\delta}$ from the expected values derived from interpolation using the mean ionic radii $\bar{r}$, it is interesting to evaluate the electrochemical performance of the air electrode layers in SOFCs, manufactured using the considered oxide. In

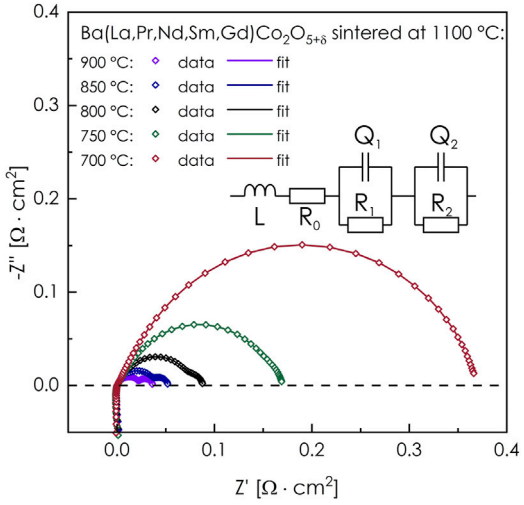

FIGURE 6
Impedance spectra collected during electrode polarization resistance measurements of (La,Pr,Nd,Sm,Gd)$BaCo_2O_{5+\delta}$ layers (manufactured on an LSGM solid electrolyte), performed with the use of the EIS method. The applied equivalent circuit is also presented. All spectra are corrected by the R_O value.

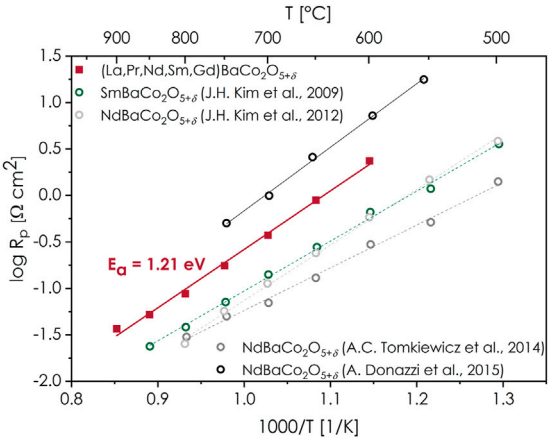

FIGURE 7
Electrode polarization resistance dependence on temperature (Arrhenius-type coordinates), determined for the layer manufactured on the LSGM solid electrolyte. The energy of activation is calculated according to Arrhenius relation: $R_p = R_{p,0} \exp(E_a/kT)$. The literature data for $NdBaCo_2O_{5+\delta}$ and $SmBaCo_2O_{5+\delta}$ are also provided (Kim et al., 2009; Kim and Irvine, 2012; Tomkiewicz et al., 2014; Donazzi et al., 2015).

order to test the feasibility of the oxide, before the symmetrical (La,Pr,Nd,Sm,Gd)$BaCo_2O_{5+\delta}$|LSGM|(La,Pr,Nd,Sm,Gd) $BaCo_2O_{5+\delta}$ cell was prepared, the inertness of the candidate cathode material toward LSGM electrolyte was established. It was done on a basis of the structural evaluation of a 50:50 wt.

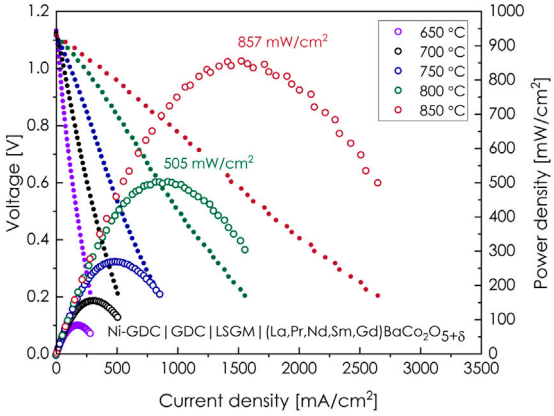

FIGURE 8
Current–voltage and power density curves recorded in a 650–850 °C temperature range for the Ni-$Ce_{0.8}Gd_{0.2}O_{2-\delta}$|$Ce_{0.8}Gd_{0.2}O_{2-\delta}$|$La_{0.8}Sr_{0.2}Ga_{0.8}Mg_{0.2}O_{3-\delta}$|(La,Pr,Nd,Sm,Gd) $BaCo_2O_{5+\delta}$ electrolyte-supported, button-type fuel cell.

ratio of a pelletized mixture of the respective powders, which was sintered for 2h at 1,100°C (corresponding to the conditions during the electrode's preparation). As can be seen in Supplementary Figure S10, no secondary phases were visible after the heat treatment, with little change in the lattice parameters, proving the stability of the electrode material. This is expected considering the already proven stability of $REBaCo_2O_{5+\delta}$ toward LSGM (Huang et al., 2018).

Regarding the electrode polarization resistance R_p, the exemplary impedance spectra of the investigated symmetrical cell can be seen in Figure 6. Based on the equivalent circuit model described in (Olszewska et al., 2018), the value of R_p could be determined. The measured spectra shape, recorded at the highest temperatures (850–900°C) suggest that both contributions of the cathodic polarization resistance, associated with the interfacial electrolyte/electrode processes and charge transfer (high-frequencies arc) and surface-related processes (low frequencies arc) are similar, but both are small. What is interesting is that the shape of the impedance curves changes with a decrease in temperature, and the increased contribution of the high-frequency arc is visible at lower temperatures, which indicates the higher activation energy of interfacial electrolyte/electrode processes. The calculated values of the electrode polarization resistance exhibit a linear dependence on temperature in log R_p-T^{-1} coordinates, as is shown in Figure 7. The established activation energy is 1.21 eV, which can be considered moderate (Zheng et al., 2012; Pelosato et al., 2014; Olszewska and Świerczek, 2019). The lowest recorded value of R_p equals to 0.037 Ω cm^2 at 900°C, while it increases to 0.175 Ω cm^2 at 750°C. While the values of cathodic polarization are strongly dependent on the cathode's microstructure, which makes a direct comparison

challenging if not impossible, it can be seen that the determined performance fits into the range of values typically reported for Nd- and Sm-based compositions, which are also shown in Figure 7 for comparison (Kim et al., 2009; Kim and Irvine, 2012; Tomkiewicz et al., 2014; Donazzi et al., 2015). Taking into account the commonly accepted limit of the R_p value equal to 0.15 Ω cm^2 (Pelosato et al., 2015), if the application is considered, the developed (La,Pr,Nd,Sm,Gd)$BaCo_2O_{5+\delta}$ layer should perform satisfactorily at and above ca. 770°C. It is likely that the performance can be further enhanced with the improvement of the electrode's morphology (e.g., by further optimization of the sintering conditions).

To further prove the possibility of utilizing the (La,Pr,Nd,Sm,Gd)$BaCo_2O_{5+\delta}$ material in SOFC technology, the electrolyte-supported, Ni-$Ce_{0.8}Gd_{0.2}O_{2-\delta}$|$Ce_{0.8}Gd_{0.2}O_{2-\delta}$|$La_{0.8}Sr_{0.2}Ga_{0.8}Mg_{0.2}O_{3-\delta}$|(La,Pr,Nd,Sm,Gd)$BaCo_2O_{5+\delta}$ button-type full cell was prepared, and its operating parameters were determined, as presented in Figure 8. As can be seen, utilization of the (La,Pr,Nd,Sm,Gd)$BaCo_2O_{5+\delta}$ cathode allows obtaining an excellent electrochemical performance, with the peak power density of 857 mW/cm^2 recorded at 850°C. Such a value, especially accounting for the fact that it was determined for the electrolyte-supported cell, further proves the high catalytic activity of the (La,Pr,Nd,Sm,Gd)$BaCo_2O_{5+\delta}$ material toward the oxygen-reduction reaction. The polished cross-section of the cell after the measurement is presented in Supplementary Figures S11, S12. Surprisingly, the EDS point analysis indicates the possibility of local instability of the system, with the elemental ratio suggesting the local presence of a simple perovskite phase. Furthermore, long-term studies of stability under the current load will be certainly necessary to address this observation. Still, it does not appear to affect the observed performance.

Based on the previously presented results, it can be stated that despite no evident high-entropy-related significant modification of the physicochemical properties of (La,Pr,Nd,Sm,Gd)$BaCo_2O_{5+\delta}$, the material shows excellent electrocatalytic activity if used to manufacture SOFC air electrodes. The application of the high-entropy approach, which does not allow obtaining the basic properties outside of the rule-of-mixtures, enables a very precise implementation of the aforementioned rule—in fact to a higher degree than in the system with only two lanthanide ions. Further studies will focus on exploring the other potential benefits of the high-entropy approach, such as the possibility of suppressing the surface segregation effects, and increasing the long-term stability of electrochemical performance, as reported in (Yang et al., 2021) and (Shen et al., 2021).

4 Conclusion

To summarize, a novel single-phase *P4/mmm*-structured high-entropy (La,Pr,Nd,Sm,Gd)$BaCo_2O_{5+\delta}$ double perovskite having a layered arrangement of the A-site cations was successfully synthesized for the first time, with the use of the soft chemistry method. The presence of a multicomponent occupancy at the A-sites seems to not affect the physicochemical properties of the material, with no obvious synergistic effects being observed. Instead, most of the studied characteristics are within the expected interpolated range based on the mean radius $\bar{r}$ of all the employed RE cations. What is more, the material appears to follow the rule-of-mixtures to an even higher degree than the more conventional $Nd_{0.88}Sm_{0.12}Co_2O_{5+\delta}$ composition, characterized by the same value of the effective ionic radius on the RE-occupied sublattice, potentially enabling a very precise design of functional properties in the double perovskite structure. The manufactured (La,Pr,Nd,Sm,Gd)$BaCo_2O_{5+\delta}$ layers (in button-type, LSGM-supported SOFC) show very low electrode polarization resistance and good performance in a full cell. Furthermore, the expected benefits of the high-entropy approach are likely to be more visible with respect to the broadly understood functionality of air-electrode materials than the electrochemical performance, e.g., by enhancing the long-term performance stability of the material or suppressing the formation of carbonate phases (Dąbrowa et al., 2017; Shen et al., 2021; Yang et al., 2021). Finally, it should be noted that the presented approach does not exhaust all the potential opportunities provided by the application of the high-entropy design principle to the synthesis of double perovskites, with the studies toward its application to the B-site position already being underway.

Data availability statement

The original contributions presented in the study are included in the article/Supplementary Material; further inquiries can be directed to the corresponding author.

Author contributions

JD: Conceptualization, Methodology, Formal analysis, Investigation, Writing—Original Draft, Writing—Review and Editing, Visualization, Supervision, Project Administration, Funding Acquisition AS: Methodology, Formal Analysis, Investigation, Resources, Visualization, Writing—Original Draft, Writing—Review and Editing MS: Methodology, Formal Analysis, Investigation, Writing—Review and Editing MZ: Methodology, Software, Data Curation, Formal Analysis, Investigation, Writing—Review and Editing PC: Methodology, Formal Analysis, Investigation, Writing—Review and Editing KŚ: Conceptualization, Formal Analysis, Resources,

Writing—Original Draft, Writing—Review and Editing, Supervision, Project Administration.

Funding

This research was supported by the Polish National Science Center (NCN) under project No. UMO-2021/41/B/ST8/04365.

Conflict of interest

The authors declare that the research was conducted in the absence of any commercial or financial relationships that could be construed as a potential conflict of interest.

Publisher's note

Supplementary material

The Supplementary Material for this article can be found online at: https://www.frontiersin.org/articles/10.3389/fenrg.2022.899308/full#supplementary-material

References

Berardan, D., Franger, S., Meena, A. K., and Dragoe, N. (2016). Room temperature lithium superionic conductivity in high entropy oxides. *J. Mat. Chem. A Mat.* 4, 9536–9541. doi:10.1039/C6TA03249D

Boaro, M. (2014). *Advances in medium and high temperature solid oxide fuel cell technology*. Berlin, Germany: Springer.

Broux, T., Bahout, M., Hanlon, J. M., Hernandez, O., Paofai, S., Berenov, A., et al. (2014). High temperature structural stability, electrical properties and chemical reactivity of $NdBaCo_{2-x}Mn_xO_{5+\delta}$ ($0 \le x \le 2$) for use as cathodes in solid oxide fuel cells. *J. Mat. Chem. A* 2 (40), 17015–17023. doi:10.1039/C4TA03364G

Dąbrowa, J., Cieslak, J., Zajusz, M., Mozdzierz, M., Berent, K., Mikula, A., et al. (2021). Structure and transport properties of the novel $(Dy, Er, Gd, Ho, Y)_3Fe_5O_{12}$ and $(Dy, Gd, Ho, Sm, Y)_3Fe_5O_{12}$ high entropy garnets. *J. Eur. Ceram. Soc.* 41 (6), 3844–3849. doi:10.1016/j.jeurceramsoc.2020.12.052

Dąbrowa, J., Olszewska, A., Falkenstein, A., Schwab, C., Szymczak, M., Zajusz, M., et al. (2020b). A innovative approach to design SOFC air electrode materials: High entropy $La_{1-x}Sr_x(Co, Cr, Fe, Mn, Ni)O_{3-\delta}$ (x = 0, 0.1, 0.2, 0.3) perovskites synthesized by the sol-gel method. *J. Mat. Chem. A Mat.* 8, 24455–24468. doi:10.1039/D0TA06356H

Dąbrowa, J., Stygar, M., Mikula, A., Knapik, A., Mroczka, K., Tejchman, W., et al. (2017). Synthesis and microstructure of the $(Co, Cr, Fe, Mn, Ni)_3O_4$ high entropy oxide characterized by spinel structure. *Mater. Lett.* 216, 32–36. doi:10.1016/j.matlet.2017.12.148

Dąbrowa, J., Szymczak, M., Zajusz, M., Mikula, A., Mozdzierz, M., Berent, K., et al. (2020a). Stabilizing fluorite structure in ceria-based high-entropy oxides: Influence of Mo addition on crystal structure and transport properties. *J. Eur. Ceram. Soc.* 40, 5870–5881. doi:10.1016/j.jeurceramsoc.2020.07.014

Djenadic, R., Sarkar, A., Clemens, O., Loho, C., Botros, M., Chakravadhanula, V. S. K., et al. (2016). Multicomponent equiatomic rare Earth oxides. *Mater. Reserch Lett.* 5, 102–109. doi:10.1080/21663831.2016.1220433

Donazzi, A., Pelosato, R., Cordaro, G., Stucchi, D., Cristiani, C., Dotelli, G., et al. (2015). Evaluation of Ba deficient $NdBaCo_2O_{5+\delta}$ oxide as cathode material for IT-SOFC. *Electrochimica Acta* 182, 573–587. doi:10.1016/j.electacta.2015.09.117

Du, Z., Yan, C., Zhao, H., Zhang, Y., Yang, C., Yi, S., et al. (2017). Effective Ca-doping in $Y_{1-x}Ca_xBaCo_2O_{5+\delta}$ cathode materials for intermediate temperature solid oxide fuel cells. *J. Mat. Chem. A Mat.* 5 (48), 25641–25651. doi:10.1039/C7TA08954F

Du, Z., Zhao, H., Shen, Y., Wang, L., Fang, M., Swierczek, K., et al. (2014). Evaluation of $La_{0.3}Sr_{0.7}Ti_{1-x}Co_xO_3$ as a potential cathode material for solid oxide fuel cells. *J. Mat. Chem. A* 2 (26), 10290–10299. doi:10.1039/C4TA00658E

Fergus, J. W. (2005). Metallic interconnects for solid oxide fuel cells. *Mater. Sci. Engineering:A* 397, 271–283. doi:10.1016/j.msea.2005.02.047

Frontera, C., Caneiro, A., Carrillo, A. E., Oro-Sole, J., and Garcia-Munoz, J. L. (2005). Tailoring oxygen content on $PrBaCo_2O_{5+\delta}$ layered cobaltites. *Chem. Mat.* 17 (22), 5439–5445. doi:10.1021/cm051148q

Gao, Z., Mogni, L. V., Miller, E. C., Railsback, J. G., and Barnett, S. A. (2016). A perspective on low-temperature solid oxide fuel cells. *Energy Environ. Sci.* 9 (5), 1602–1644. doi:10.1039/C5EE03858H

Goodenough, J. B. (1958). An interpretation of the magnetic properties of the perovskite-type mixed crystals $La_{1-x}Sr_xCoO_{3-\lambda}$. *J. Phys. Chem. Solids* 6 (2–3), 287–297. doi:10.1016/0022-3697(58)90107-0

Han, X., Yang, Y., Fan, Y., Ni, H., Guo, Y., Chen, Y., et al. (2021). New approach to enhance Sr-free cathode performance by high-entropy multi-component transition metal coupling. *Ceram. Int.* 47 (12), 17383–17390. doi:10.1016/j.ceramint.2021.03.052

Huang, X., Feng, J., Abdellatif, H. R., Zou, J., Zhang, G., and Ni, C. (2018). Electrochemical evaluation of double perovskite $PrBaCo_{2-x}Mn_xO_{5+\delta}$ (x = 0, 0.5, 1) as promising cathodes for IT-SOFCs. *Int. J. Hydrogen Energy* 43 (18), 8962–8971. doi:10.1016/j.ijhydene.2018.03.163

Hwang, J., Rao, R. R., Giordano, L., Katayama, Y., Yu, Y., and Shao-Horn, Y. (2017). Perovskites in catalysis and electrocatalysis. *Science* 358 (6364), 751–756. doi:10.1126/science.aam7092

Ishihara, T. (2014). *Perovskite Oxide for soild oxide fuel cells*. New York: Springer.

Karppinen, M., Matvejeff, M., Salomaki, K., and Yamauchi, H. (2002). Oxygen content analysis of functional perovskite-derived cobalt oxides. *J. Mat. Chem.* 12 (6), 1761–1764. doi:10.1039/b200770n

Kim, J.-H., and Manthiram, A. (2015). Layered $LnBaCo_2O_{5+\delta}$ perovskite cathodes for solid oxide fuel cells: An overview and perspective. *J. Mat. Chem. A* 3 (48), 24195–24210. doi:10.1039/C5TA06212H

Kim, J.-H., and Manthiram, A. (2008). $LnBaCo_2O_{5+\delta}$ oxides as cathodes for intermediate-temperature solid oxide fuel cells. *J. Electrochem. Soc.* 155 (4), B385. doi:10.1149/1.2839028

Kim, J.-H., Mogni, L., Prado, F., Caneiro, A., Alonso, J. A., and Manthiram, A. (2009a). High temperature crystal chemistry and oxygen permeation properties of the mixed ionic–electronic conductors $LnBaCo_2O_{5+\delta}$ (Ln=Lanthanide). *J. Electrochem. Soc.* 156 (12), B1376. doi:10.1149/1.3231501

Kim, J., Choi, S., Park, S., Kim, C., Shin, J., and Kim, G. (2013). Effect of Mn on the electrochemical properties of a layered perovskite $NdBa_{0.5}Sr_{0.5}Co_{2-x}Mn_xO_{5+\delta}$ (x = 0, 0.25, and 0.5) for intermediate-temperature solid oxide fuel cells. *Electrochimica Acta* 112, 712–718. doi:10.1016/j.electacta.2013.09.014

Kim, J. H., and Irvine, J. T. S. (2012). Characterization of layered perovskite oxides $NdBa_{1-x}Sr_xCo_2O_{5+\delta}$ (x = 0 and 0.5) as cathode materials for IT-SOFC. *Int. J. Hydrogen Energy* 37 (7), 5920–5929. doi:10.1016/j.ijhydene.2011.12.150

Kim, J. H., Kim, Y., Connor, P. A., Irvine, J. T., Bae, J., and Zhou, W. (2009b). Structural, thermal and electrochemical properties of layered perovskite $SmBaCo_2O_{5+\delta}$, a potential cathode material for intermediate-temperature solid oxide fuel cells. *J. Power Sources* 194 (2), 704–711. doi:10.1016/j.jpowsour.2009.06.024

Kim, J. P., Pyo, D. W., Magnone, E., and Park, J. H. (2012). Preparation and oxygen permeability of $ReBaCo_2O_{5+\delta}$ (Re = Pr, Nd, Y) ceramic membranes. *Adv. Mat. Res.* 560–561, 959–964. doi:10.4028/www.scientific.net/AMR.560-561.959

Kong, X. (2018). Effect of Mn on the characterization of layered perovskite $NdBaCo_{2-x}Mn_xO_{5+\delta}$ (x=0.5, 1, 1.5, 2) as cathode materials for IT- SOFCs. *Int. J. Electrochem. Sci.* 13, 7939–7948. doi:10.20964/2018.08.68

Kübel, C., Velasco, L., Wang, D., Wang, Q., Talasila, G., de Biasi, L., et al. (2018). High entropy oxides for reversible energy storage. *Nat. Commun.* 9, 3400. doi:10.1038/s41467-018-05774-5

Larminie, A., and Dicks, A. (2003). *Fuel cell systems explained*. New York, United States: John Wiley & Sons.

Lee, H. Y., Huang, K., and Goodenough, J. B. (1998). Sr- and Ni-doped $LaCoO_3$ and $LaFeO_3$ perovskites. *J. Electrochem. Soc.* 145 (9), 3220–3227. doi:10.1149/1.1838789

Li, F., Zhou, L., Liu, J. X., Liang, Y., and Zhang, G. J. (2019). High-entropy pyrochlores with low thermal conductivity for thermal barrier coating materials. *J. Adv. Ceram.* 8 (3), 576–582. doi:10.1007/s40145-019-0342-4

Liu, S., Zhang, W., Li, Y., and Yu, B. (2017). $REBaCo_2O_{5+\delta}$ (RE = Pr, Nd, and Gd) as promising oxygen electrodes for intermediate-temperature solid oxide electrolysis cells. *RSC Adv.* 7 (27), 16332–16340. doi:10.1039/C6RA28005F

Mahato, N., Banerjee, A., Gupta, A., Omar, S., and Balani, K. (2015). Progress in material selection for solid oxide fuel cell technology: A review. *Prog. Mater. Sci.* 72, 141–337. doi:10.1016/j.pmatsci.2015.01.001

Miracle, D. B., and Senkov, O. N. (2016). A critical review of high entropy alloys and related concepts. *Acta Mater.* 122, 448–511. doi:10.1016/j.actamat.2016.08.081

Mogni, L., Prado, F., Jimenez, C., and Caneiro, A. (2013). Oxygen order-disorder phase transition in layered $GdBaCo_2O_{5+\delta}$ perovskite: Thermodynamic and transport properties. *Solid State Ionics* 240, 19–28. doi:10.1016/j.ssi.2013.03.021

Muñoz-Gil, D., Perez-Coll, D., Pena-Martinez, J., and Garcia-Martin, S. (2014). New insights into the $GdBaCo_2O_{5+\delta}$ material: Crystal structure, electrical and electrochemical properties. *J. Power Sources* 263, 90–97. doi:10.1016/j.jpowsour.2014.04.019

Olszewska, A., Du, Z., Swierczek, K., Zhao, H., and Dabrowski, B. (2018). Novel $ReBaCo_{1.5}Mn_{0.5}O_{5+\delta}$ (Re: La, Pr, Nd, Sm, Gd and Y) perovskite oxide: Influence of manganese doping on the crystal structure, oxygen nonstoichiometry, thermal expansion, transport properties, and application as a cathode material for solid oxide fuel cells. *J. Mat. Chem. A Mat.* 6, 13271–13285. doi:10.1039/C8TA03479F

Olszewska, A., and Świerczek, K. (2019). $ReBaCo_{2-x}Mn_xO_{5+\delta}$ (Re: Rare Earth element) layered perovskites for application as cathodes in solid oxide fuel cells. *E3S Web Conf.* 108, 01020. doi:10.1051/e3sconf/201910801020

Olszewska, A., Swierczek, K., Skubida, W., Du, Z., Zhao, H., and Dabowski, B. (2019). Versatile application of redox processes for $REBaCoMnO_{5+\delta}$ (RE: La, Pr, Nd, Sm, Gd, and Y) oxides. *J. Phys. Chem. C* 123, 48–61. doi:10.1021/acs.jpcc.8b08585

Olszewska, A., Zhang, Y., Du, Z., Marzec, M., Swierczek, K., Zhao, H., et al. (2019). Mn-rich $SmBaCo_{0.5}Mn_{1.5}O_{5+\delta}$ double perovskite cathode material for SOFCs. *Int. J. Hydrogen Energy* 44 (50), 27587–27599. doi:10.1016/j.ijhydene.2019.08.254

Pelosato, R., Cordaro, G., Stucchi, D., Cristiani, C., and Dotelli, G. (2015). Cobalt based layered perovskites as cathode material for intermediate temperature solid oxide fuel cells: A brief review. *J. Power Sources* 298, 46–67. doi:10.1016/j.jpowsour.2015.08.034

Pelosato, R., Donazzi, A., Dotelli, G., Cristiani, C., Natali Sora, I., and Mariani, M. (2014). Electrical characterization of co-precipitated $LaBaCo_2O_{5+\delta}$ and $YBaCo_2O_{5+\delta}$ oxides. *J. Eur. Ceram. Soc.* 34 (16), 4257–4272. doi:10.1016/j.jeurceramsoc.2014.07.005

Ramadhani, F., Hussain, M., Mokhlis, H., and Hajimolana, S. (2017). Optimization strategies for solid oxide fuel cell (SOFC) application : A literature survey. *Renew. Sustain. Energy Rev.* 76, 460–484. doi:10.1016/j.rser.2017.03.052

Raveau, B., and Seikh, M. (2012). *Crystal chemistry of cobalt oxides*. Weinheim, Germany: Wiley-VCH Verlag GmbH & Co. KGaA.

Sengodan, S., Choi, S., Jun, A., Shin, T. H., Ju, Y. W., Jeong, H. Y., et al. (2015). Layered oxygen-deficient double perovskite as an efficient and stable anode for direct hydrocarbon solid oxide fuel cells. *Nat. Mat.* 14 (2), 205–209. doi:10.1038/nmat4166

Shannon, R. D. (1976). Revised effective ionic radii and systematic studies of interatomic distances in halides and chalcogenides. *Acta Cryst. Sect. A* A32, 751–767. doi:10.1107/s0567739476001551

Shen, L., Du, Z., Zhang, Y., Dong, X., and Zhao, H. (2021). Medium-Entropy perovskites $Sr(Fe_\alpha Ti_\beta Co_\gamma Mn_\zeta)O_{3-\delta}$ as promising cathodes for intermediate temperature solid oxide fuel cell. *Appl. Catal. B Environ.* 295, 120264. doi:10.1016/j.apcatb.2021.120264

Staffell, I., Scamman, D., Velazquez Abad, A., Balcombe, P., Dodds, P. E., Ekins, P., et al. (2019). The role of hydrogen and fuel cells in the global energy system. *Energy Environ. Sci.* 12 (2), 463–491. doi:10.1039/c8ee01157e

Sun, C., Hui, R., and Roller, J. (2010). Cathode materials for solid oxide fuel cells: A review. *J. Solid State Electrochem.* 14, 1125–1144. doi:10.1007/s10008-009-0932-0

Tomkiewicz, A. C., Meloni, M., and McIntosh, S. (2014). On the link between bulk structure and surface activity of double perovskite based SOFC cathodes. *Solid State Ionics* 260, 55–59. doi:10.1016/j.ssi.2014.03.015

Tseng, K. P., Mccormack, S. J., and Kriven, W. M. (2019). High-entropy, phase-constrained, lanthanide sesquioxide. *J. Am. Ceram. Soc.* 103, 569–576. doi:10.1111/jace.16689

Tsvetkov, D. S., Ivanov, I., Urusov, I., and Zuev, A. (2011). Thermodynamics of formation of double perovskites $GdBaCo_{2-x}M_xO_{6-\delta}$ (M = Fe, Mn; X = 0, 0.2). *Thermochim. Acta* 519 (1–2), 12–15. doi:10.1016/j.tca.2011.02.022

Tsvetkov, D. S., Sereda, V. V., and Zuev, A. Y. (2016). Oxygen nonstoichiometry and electrochemical properties of GdBaCo2-xFexO6-d double perovskite cathodes. *Ural Fed. Univ. Res. portal* 8, 6–9. doi:10.1115/1.4003631

Vinnik, D. A., Trofimov, E. A., Zhivulin, V. E., Zaitseva, O. V., Gudkova, S. A., Starikov, A. Y., et al. (2019). High-entropy oxide phases with magnetoplumbite structure. *Ceram. Int.* 45, 12942–12948. doi:10.1016/j.ceramint.2019.03.221

Volkova, N. E., Gavrilova, L., Cherepanov, V., Aksenova, T., Kolotygin, V., and Kharton, V. (2013). Synthesis, crystal structure and properties of $SmBaCo_{2-x}Fe_xO_{5+\delta}$. *J. Solid State Chem.* 204, 219–223. doi:10.1016/j.jssc.2013.06.001

Yang, Y., Bao, H., Ni, H., Ou, X., Wang, S., Lin, B., et al. (2021). A novel facile strategy to suppress Sr segregation for high-entropy stabilized $La_{0.8}Sr_{0.2}MnO_{3-\delta}$ cathode. *J. Power Sources* 482, 228959. doi:10.1016/j.jpowsour.2020.228959

Zhang, K., Ge, L., Ran, R., Shao, Z., and Liu, S. (2008). Synthesis, characterization and evaluation of cation-ordered $LnBaCo_2O_{5+\delta}$ as materials of oxygen permeation membranes and cathodes of SOFCs. *Acta Mater.* 56 (17), 4876–4889. doi:10.1016/j.actamat.2008.06.004

Zhang, Y., Krylov, D., Rosenkranz, M., Schiemenz, S., and Popov, A. A. (2015). Magnetic anisotropy of endohedral lanthanide ions: Paramagnetic NMR study of $MSc_2N@C80$-ih with M running through the whole 4f row. *Chem. Sci.* 6, 2328–2341. doi:10.1039/C5SC00154D

Zhang, Y. (2004). *History of high entropy oxides*. Singapore: Spronger Nature Pte Ltd.

Zhang, Y., Zhao, H., Du, Z., Swierczek, K., and Li, Y. (2019). High performance $SmBaMn_2O_{5+\delta}$ electrode for symmetrical solid oxide fuel cell. *Chem. Mat.* 31, 3784–3793. doi:10.1021/acs.chemmater.9b01012

Zhao, C., Ding, F., Lu, Y., Chen, L., and Hu, Y. (2020). High-entropy layered oxide cathodes for sodium-ion batteries. *Angew. Chem. Int. Ed.* 59 (1), 264–269. doi:10.1002/anie.201912171

Zhao, H., Zheng, Y., Yang, C., Shen, Y., Du, Z., and Swierczek, K. (2013). Electrochemical performance of $Pr_{1-x}Y_xBaCo_2O_{5+\delta}$ layered perovskites as cathode materials for intermediate-temperature solid oxide fuel cells. *Int. J. Hydrogen Energy* 38 (36), 16365–16372. doi:10.1016/j.ijhydene.2013.10.003

Zhao, L., Chen, K., Liu, Y., and He, B. (2017). A novel layered perovskite as symmetric electrode for direct hydrocarbon solid oxide fuel cells. *J. Power Sources* 342, 313–319. doi:10.1016/j.jpowsour.2016.12.066

Zheng, K., Gorzkowska-Sobaś, A., and Świerczek, K. (2012). Evaluation of Ln_2CuO_4(ln: La, Pr, Nd) oxides as cathode materials for IT-SOFCs. *Mater. Res. Bull.* 47 (12), 4089–4095. doi:10.1016/j.materresbull.2012.08.072